

Received June 1, 2021, accepted June 15, 2021, date of publication June 29, 2021, date of current version July 13, 2021.

Digital Object Identifier 10.1109/ACCESS.2021.3093351

One-Step-Prediction Discrete Observer Based Frequency-Locked-Loop Technique for Three-Phase System

WEI HU¹, YAODONG WU^{1,2}, YU SHEN¹, FAN YANG¹, XIANGJUN QUAN², (Member, IEEE), FUJIN DENG^{1,2}, (Senior Member, IEEE), AND ZHIXIANG ZOU^{1,2}, (Senior Member, IEEE)

¹Electric Power Research Institute, State Grid Hubei Electric Power Company, Wuhan 430077, China

²School of Electrical Engineering, Southeast University, Nanjing 210018, China

Corresponding author: Yaodong Wu (1067766378@qq.com)

This work was supported by the Project of State Grid Hubei Electric Power Company Ltd under Grant 521532200020.


ABSTRACT In grid-tied power converters, the grid parameters such as the frequency, phase angle of the fundamental component, and the harmonics are essential to the control of power converters, the fast and accurate estimation of the grid parameters is a challenge especially for high-order harmonics. This paper proposes a one-step-prediction (OSP) discrete observer (OSPDO) to observe the fundamental and harmonic sequence components of the grid voltage. Based on the proposed OSPDO, a frequency locked loop (FLL) is designed. The proposed OSPDO-FLL has a good robustness to sampling frequency on dynamic response and high precision for frequency estimation. The proposed algorithm can estimate up to maximum 50th harmonic with a low sampling frequency thanks to the robust properties. Finally, the good characteristics of the proposed synchronization algorithm are verified by simulations and laboratory experiments.

INDEX TERMS One-step prediction, frequency locked loop, adaptive state observer, harmonic detection, grid synchronization.

I. INTRODUCTION

The distributed generations are playing important roles in the electric grids all over the world. In the distributed scenario, electricity networks of the future will have a high penetration of power electronic devices as an interface between the generation systems and the grid. The synchronization with the voltage at the point of common coupling (PCC) is a key prerequisite in the realization of the power converters connected to the grid [1], [2].

The most popular grid synchronization techniques are phase-locked loops (PLLs) [1], [3]–[6] and frequency locked loops (FLLs) [2], [9]–[19]. The PLL and FLL techniques are not only simple to implement on a real-time DSP and can also provide instantaneous estimation of the grid voltage parameters and harmonics. The biggest distinctions between the PLL and FLL are the application background and feedback variable. The PLL generally provides an accurate phase angle estimation (the phase angle is the feedback variable)

The associate editor coordinating the review of this manuscript and approving it for publication was Wonhee Kim .

for the control of the power converter under a synchronous reference frame (SRF) where a Park transformation is the prerequisite. In contrast, the FLL offers a precise estimation of the fundamental frequency (the frequency is the feedback variable) for resonant controllers of the power converter under the stationary reference frame, where the precision of the frequency is very important. Because small frequency variation will result in the steady-state error and the phase delay for the sinusoidal signal tracking control.

The synchronous reference frame phase locked loop (SRF-PLL) has been a traditional synchronization technique for grid voltage and has been widely applied in the control of grid-tied converters [3], [4]. A lot of efforts have been dedicated to the PLL techniques under distorted grid conditions and numerous synchronization algorithms are developed with excellent performance [3]–[6]. A decoupled network is adopted to eliminate the influence of negative sequence components in [3]. A single-phase PLL is proposed in [4] based on a second-order generalized integrator (SOGI) which is used to generate the in-phase and orthogonal signals. A nonlinear active disturbance rejection loop filter is proposed for the

PLL to achieve a good performance. The linear time-periodic model is established in [6] to analyze and improve the performance of the PLL. Generally, the improvement of the PLL mainly focuses on the prefilter and the in-loop filter [1]. More information concerning the advanced PLL can refer [1].

References [7]–[19] focus on the advanced FLL techniques, which can also estimate the harmonic components. On the basis of the research in [9]–[17], lots of improved FLLs were developed based on continuous-time adaptive filters, including the adaptive vectorial filter (AVF-FLL) [7], reduced-order generalized integrator (ROGI-FLL) [8], and the second-order generalized integrator (SOGI-FLL) [9]–[12] for frequency estimation and harmonic detection. A modified SOGI is proposed in [12] with additional control gain, so that the real parts of the poles can be chosen arbitrarily. The increased control degree of the freedom (DOF) improves the dynamic response of the SOGI. A reduced order observer which only adopts three state variables is proposed in [14] for estimating grid voltage fundamental positive and negative sequences and frequency. The Popov's MRAC approach is adopted in [15] to generalize the framework of the FLL design. The proportional-integral-based FLL is recommended in [15]. Later, the proportional-integral-based FLL is further modelled in [16] and [17] to achieve a better dynamic response in synchronized reference frame than conventional FLL. In [18], the repetitive controller is employed to replace the SOGI, so that the implementation of the FLL becomes simpler. While in [19], the direct transfer delay link is used to generate the in-phase and orthogonal signals of the input voltage.

Although these advanced continuous time FLL techniques demonstrate an outstanding performance on frequency estimation and harmonic detection, their estimation precision and response performance highly depend on the discretization method and sampling frequency [20]–[23]. The better choice is to design the FLL in discrete-time domain as in [13] and [23]. In [13], a discrete-time algorithm is designed directly in discrete-time domain to achieve a good estimation performance. A straightforward discrete-time filter without feedback loop is proposed to design the FLL in [23]. Furthermore, in grid-tied applications, the grid regulations require fast transient responses [10], [11], and in some grid standards, the maximum 50th harmonic component is specified [24]. Besides that, in aircraft AC power system, up to 360-900 Hz signals often needs to be estimated [25], the estimation for such a high frequency usually requires a high sampling frequency according to Nyquist sampling theory. In this condition, the low ratio between the sampling frequency and the signal frequency has to be faced in the implementation of the synchronization algorithm. It increases the difficulty to select the suitable sampling frequency. Therefore, it is important to develop an algorithm that can estimate the high frequency signal with a non-exorbitant sampling frequency (less sampled points in one period of the input signal). A high performance in low sampling frequency is achieved by the method in [23]. However, the error signal is absence in the

FLL due to the straightforward implementation [23], which increases the difficulties for the FLL, since the error signal is generally used as the input of the frequency estimation loop. Moreover, the stability is not analyzed in [23].

To develop an algorithm which has good dynamic and steady state performance with low sampling frequency, a one-step-prediction (OSP) discrete observer (OSPDO) based frequency locked loop (OSPDO-FLL) is proposed in this paper. Compared with the method in [23], the feedback structure is employed, consequently, the error signal is available which is benefit for the implementation of the FLL. Furthermore, the improved stability of the OSPDO is analyzed in this paper. The parameter design for multiple OSPDO is also demonstrated. The analysis indicates that the proposed algorithm can demonstrate good robust properties to sampling frequency. The good performance of the proposed algorithm is finally verified by the simulations and experiments.

II. ONE-STEP PREDICTION DISCRETE OBSERVER

A. OBSERVER FOR SINGLE SEQUENCE COMPONENT

It is well-known that the three-phase fundamental positive sequence fundamental grid voltage can be expressed as following equation in the $\alpha\beta$ stationary reference frame:

$$\mathbf{v}_{\alpha\beta}^{(+1)} = \begin{bmatrix} V^{(+1)} \cos(\omega t) \\ V^{(+1)} \sin(\omega t) \end{bmatrix} \quad (1)$$

where $\omega = 2\pi f$ is the angle frequency and f is the fundamental frequency, and $V^{(+1)}$ is the amplitude. Then the dynamic characteristics of $\mathbf{v}_{\alpha\beta}^{(+1)}$ can be formulated as:

$$\frac{d\mathbf{v}_{\alpha\beta}^{(+1)}}{dt} = \begin{bmatrix} -\omega V^{(+1)} \sin(\omega t) \\ \omega V^{(+1)} \cos(\omega t) \end{bmatrix} = \begin{bmatrix} 0 & -\omega \\ \omega & 0 \end{bmatrix} \mathbf{v}_{\alpha\beta}^{(+1)} = \mathbf{A} \mathbf{v}_{\alpha\beta}^{(+1)}$$

$$\mathbf{y} = \mathbf{v}_{\alpha\beta}^{(+1)}, \mathbf{v}_{\alpha\beta,0}^{(+1)} = \mathbf{v}_{\alpha\beta}^{(+1)}(0) \quad (2)$$

where $\mathbf{y} = \mathbf{v}_{\alpha\beta}^{(+1)}$ is the output of the three-phase voltage in form of sequence component when single sequence component is considered, and $\mathbf{v}_{\alpha\beta,0}^{(+1)}$ is the initial values that includes the initial phase information. Discretizing (2) with sampling frequency $f_s = 1/T_s > 0$, T_s is the sampling time, the following discrete-time state space model is obtained as:

$$\mathbf{v}_{\alpha\beta,k+1}^{(+1)} = \begin{bmatrix} \cos(\omega T_s) & -\sin(\omega T_s) \\ \sin(\omega T_s) & \cos(\omega T_s) \end{bmatrix} \mathbf{v}_{\alpha\beta,k}^{(+1)} = \mathbf{G}(\omega T_s) \mathbf{v}_{\alpha\beta,k}^{(+1)}$$

$$\mathbf{y}_k = \mathbf{v}_{\alpha\beta,k}^{(+1)}, \mathbf{v}_{\alpha\beta,0}^{(+1)} = \mathbf{v}_{\alpha\beta}^{(+1)}(0) \quad (3)$$

in which the subscript k indicates the sampling point, and the transition matrix $\mathbf{G}(\omega T_s)$ is derived by

$$\mathbf{G}(\omega T_s) = e^{\mathbf{A}T_s} = \begin{bmatrix} \cos(\omega T_s) & -\sin(\omega T_s) \\ \sin(\omega T_s) & \cos(\omega T_s) \end{bmatrix}. \quad (4)$$

From the perspective of the state observer, as shown in **FIGURE 1** (a), the conventional observer can be designed as

$$\hat{\mathbf{v}}_{\alpha\beta,k+1}^{(+1)} = \mathbf{G}(\omega T_s) \hat{\mathbf{v}}_{\alpha\beta,k}^{(+1)} + \mathbf{M}(\omega T_s) (\mathbf{v}_{\alpha\beta,k}^{(+1)} - \hat{\mathbf{v}}_{\alpha\beta,k}^{(+1)})$$

$$\hat{\mathbf{y}}_{c,k} = \hat{\mathbf{v}}_{\alpha\beta,k}^{(+1)} \quad (5)$$

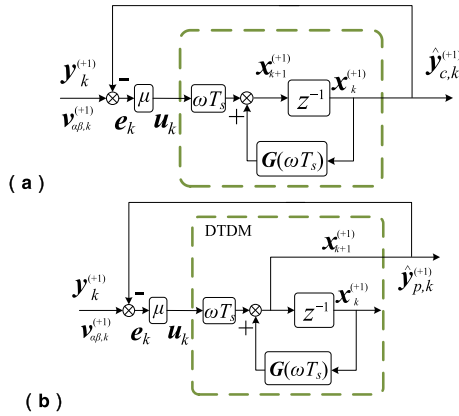


FIGURE 1. (a) Conventional observer; (b) proposed OSPDO.

where $M(\omega T_s)$ is the matrix gain and the term $\hat{y}_{c,k} = \hat{v}_{\alpha\beta,k}^{(+1)}$ is the estimate of the input voltage. Differently, in this paper, the one-step prediction term $\hat{v}_{\alpha\beta,k+1}^{(+1)}$ is designed as the estimation of the input voltage. Consequently, a novel discrete observer is proposed for the positive sequence voltage $v_{\alpha\beta}^{(+1)}$ as:

$$\begin{aligned} \hat{v}_{\alpha\beta,k+1}^{(+1)} &= G(\omega T_s) \hat{v}_{\alpha\beta,k}^{(+1)} + M(\omega T_s) (v_{\alpha\beta,k}^{(+1)} - \hat{v}_{\alpha\beta,k+1}^{(+1)}) \\ \hat{y}_{p,k} &= \hat{v}_{\alpha\beta,k+1}^{(+1)} \end{aligned} \quad (6)$$

where $M(\omega T_s)$ is the matrix gain and the one-step prediction $\hat{y}_{p,k} = \hat{v}_{\alpha\beta,k+1}^{(+1)}$ is adopted as the estimate of $v_{\alpha\beta,k}^{(+1)}$. Generally, the matrix gain is helpful for the dynamic improvement for SOGI [12], and the matrix gain is also adopted in [8]. However, it is pointed out in [26] that the matrix gain will occur the coupling between the amplitude and frequency estimation for ROGI-FLL. Moreover, the matrix gain hinders the solution of the algebraic loop in (6). Hence, the parameter is designed as

$$M(\omega T_s) = \mu \omega T_s I_2 \quad (7)$$

where I_2 is the identity matrix. Then, solving (6), the ultimate observer becomes

$$\hat{v}_{\alpha\beta,k+1}^{(+1)} = \frac{G(\omega T_s)}{1 + \mu \omega T_s} \hat{v}_{\alpha\beta,k}^{(+1)} + \frac{\mu \omega T_s}{1 + \mu \omega T_s} v_{\alpha\beta,k}^{(+1)} \quad (8)$$

Defining $\hat{v}_{\alpha\beta,k}^{(+1)} = \hat{x}_k^{(+1)}$ and $u_k = \mu e_k = \mu (y_k - \hat{y}_{p,k}^{(+1)})$, a discrete-time dynamic model (DTDM) in (6) can be extracted with a normalized form as shown in FIGURE 1 (b). Then, the one-step prediction discrete observer (OSPDO) is a closed-loop feedback of the DTDM, however, the feedback variable is the one-step prediction term. The transfer functions (TFs) of the DTDMs for OSPDO and conventional observer can be derived as:

$$\begin{aligned} T_p(z, \omega T_s) &= \frac{\hat{y}_k^{(+1)}}{u_k} = \omega T_s (G(zI - G)^{-1} + I) \\ &= \frac{\omega T_s}{z^2 - 2z \cos(\omega T_s) + 1} \\ &\quad \times \begin{bmatrix} z^2 - z \cos(\omega T_s) & -z \sin(\omega T_s) \\ z \sin(\omega T_s) & z^2 - z \cos(\omega T_s) \end{bmatrix} \end{aligned} \quad (9)$$

$$\begin{aligned} T_c(z, \omega T_s) &= \frac{\hat{y}_k^{(+1)}}{u_k} = \omega T_s (zI - G)^{-1} \\ &= \frac{\omega T_s}{z^2 - 2z \cos(\omega T_s) + 1} \\ &\quad \times \begin{bmatrix} z - \cos(\omega T_s) & -\sin(\omega T_s) \\ \sin(\omega T_s) & z - \cos(\omega T_s) \end{bmatrix} \end{aligned} \quad (10)$$

where z is the Z transform variable. Using complex variables, those transfer functions can be further derived as:

$$T_p(z, \omega T_s) = \frac{\omega T_s z}{z - e^{j\omega T_s}} \quad (11)$$

$$T_c(z, \omega T_s) = \frac{\omega T_s}{z - e^{j\omega T_s}} \quad (12)$$

B. OBSERVER FOR MULTIPLE SEQUENCE COMPONENTS

In practice, the voltage always contains harmonics, consequently the dynamic of the three-phase voltage can be expressed as (13), as shown at the bottom of the next page: where the output of the voltage is the superposition of the harmonics and DC component [27], [28]. Considering the harmonic property of three-phase system: the balanced condition harmonic sequences are $\dots, -11, -5, +1, +7, \dots, 6n+1$, with $n = \dots, -2, -1, 0, 1, 2, \dots$, and the unbalanced condition harmonic sequences are $\dots, -13, -7, -1, +5, +11, -13, \dots, 6n-1$, hence, the order m can be deployed as $-11, -5, -1, 0, +1, +7$ [11]. Therefore, the DTDM with harmonic digital angular frequency $m\omega T_s$

$$\text{DTDM}[G(m\omega T_s)] = \frac{|m| \omega T_s z}{z - e^{jm\omega T_s}} \quad (14)$$

can be used to estimate the harmonic sequence components with the structure shown in FIGURE 2 [28]. To make the figure more concise, the term $\hat{y}_k^{(+1)}$ is used to replace $\hat{y}_{p,k}^{(m)}$. When $m = 0$, the $\text{DTDM}[G(0\omega T_s)] = I_2$ results in

$$v_{\alpha\beta,k+1}^{(0)} = v_{\alpha\beta,k}^{(0)} \quad (15)$$

which represents the dynamic of DC signal, hence it is used in FIGURE 2 to address the DC offset [28].

C. SOLUTION OF ALGEBRAIC LOOP WITH HARMONIC ESTIMATION

It is worth noting that there is an algebraic loop between the error signal e_k and the output y_k . In case of multiple DTDMs, the algebraic loop equation can be obtained as

$$\begin{aligned} \hat{y}_k &= \sum_m \hat{y}_k^{(m)} \\ &= \sum_m \left(G(m\omega T_s) \hat{x}_k^{(m)} + \mu_m |m| \omega T_s (v_{\alpha\beta,k} - \hat{y}_k) \right) \end{aligned} \quad (16)$$

Solving \hat{y}_k from (16)

$$\hat{y}_k = \frac{\left(\omega T_s \sum_m \mu_m |m| \right) v_{\alpha\beta,k} + \sum_m \left(G(m\omega T_s) \hat{x}_k^{(m)} \right)}{1 + \omega T_s \sum_m \mu_m |m|} \quad (17)$$

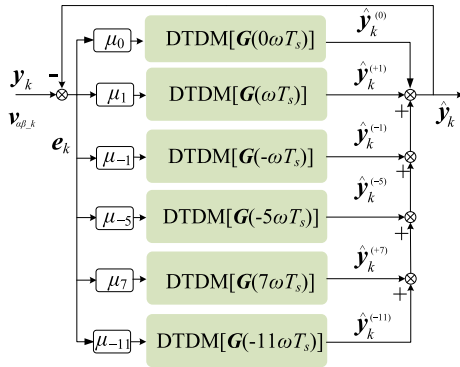


FIGURE 2. Block diagram of the harmonic observer.

then, e_k is calculated by

$$e_k = v_{\alpha\beta,k} - \hat{y}_k = \frac{v_{\alpha\beta,k} - \sum_m \left(G(m\omega T_s) \hat{x}_k^{(m)} \right)}{1 + \omega T_s \sum_m \mu_m |m|} \quad (18)$$

among which the term $G(m\omega T_s) \hat{x}_k^{(m)}$ should be computed at first. Then, e_k can be obtained from (18), and the reconstruction of harmonics can be computed by

$$\hat{y}_k^{(m)} = G(m\omega T_s) \hat{x}_k^{(m)} + \mu_m |m| \omega T_s e_k \quad (19)$$

In (18), the division term may introduce some computational burden which will be addressed later.

D. PERFORMANCE ANALYSIS

From (11) and (12), it can be found that the two complex variables transfer functions have a common feature that they own the same pole at $e^{j\omega T_s}$. This feature makes the two DTDMs have infinite gain at the positive frequency ω , which guarantees the zero-steady-state-error estimation of the positive sequence of the input voltage signal. Nevertheless, the transfer functions own different zeroes, which will affect the performance of the corresponding closed-loop observers.

To further analyze the performance of the proposed observer, we define $n = f_s/f$. Then the bode diagrams of T_p and T_c with different n are shown in FIGURE 3. As shown in FIGURE 3, both T_p and T_c have the same magnitude response which make they can achieve the zero-steady-state-error estimation of the input voltage. However, the different phase features result in different stabilities for T_p and T_c . The phase of the proposed OSPDO T_p always

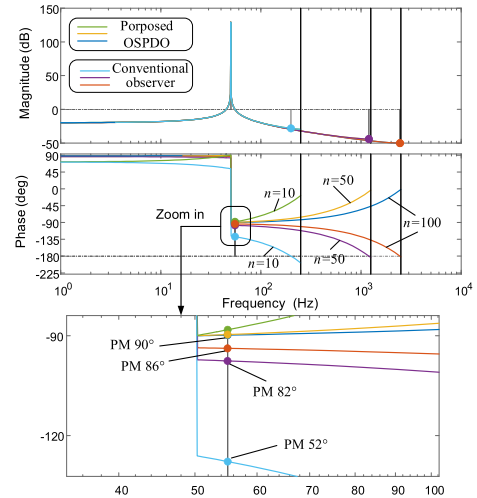


FIGURE 3. Comparison bode diagram of T_p and T_c with different n .

less than 180° regardless of n which leads in an infinite amplitude margin (AM). Nevertheless, with the reduction of n , the phase of T_c exceeds 180° which will reduce the stability (the AM will not be infinite as shown by the magnitude response). Moreover, the phase margin (PM) of the conventional observer also reduces remarkably with the reduction of n as shown in the zoom in figure. Therefore, the proposed OSPDO has stronger robustness against the sampling frequency.

E. SELECTION OF THE PARAMETERS

According to FIGURE 1 (b) and (11), the closed-loop eigenvalue of the OSPDO can be calculated as:

$$\lambda_1 = (1 + \mu\omega T_s)^{-1} e^{j\omega T_s} \quad (20)$$

From (20), it can be deduced that the dynamic response of the OSPDO is highly related with the coefficient μ . Defining $(1 + \mu\omega T_s)^{-1} = e^{-\delta T_s}$, the settling time within 2% steady error can be approximated as

$$\tau_{set} \approx \frac{-4T_s}{\ln(e^{-\delta T_s})} = \frac{4}{\delta} \quad (21)$$

Therefore, the tuning of μ for single IM is straightforward.

In multiple DTDMs condition, the setting of μ_m , which determines the dynamic performance of m -order harmonic estimation, should be done with consideration of the inter-

$$\begin{bmatrix} v_{\alpha\beta,k+1}^{(0)} \\ v_{\alpha\beta,k+1}^{(+1)} \\ \vdots \\ v_{\alpha\beta,k+1}^{(m)} \end{bmatrix} = \begin{bmatrix} G(0\omega T_s) & & & \\ & G(\omega T_s) & & \\ & & \ddots & \\ & & & G(m\omega T_s) \end{bmatrix} \begin{bmatrix} v_{\alpha\beta,k}^{(0)} \\ v_{\alpha\beta,k}^{(+1)} \\ \vdots \\ v_{\alpha\beta,k}^{(m)} \end{bmatrix}$$

$$\hat{y}_k = v_{\alpha\beta,k} = \sum_m v_{\alpha\beta,k}^{(m)}, \quad m = 0, \pm 1, \pm 2, \pm 3, \dots \quad (13)$$

action influence of each DTDMs, and the root locus method is adopted to study this issue.

FIGURE 4 shows three representative root locus plots with different varying parameters, where λ_m represents the pair of characteristic roots of m -order DTDM. From **FIGURE 4** it can be concluded that the harmonic DTDMs ($m = -11, -5, 7$) impose little influence on fundamental DTDMs ($m = \pm 1$) and vice versa. However, the fundamental positive and negative sequence components affect each other remarkably. When μ_{+1} is varying, λ_{-1} moves evidently, and λ_1 moves with μ_{-1} varying as well. Hence the set for negative sequence component should be careful. The corresponding accepted zones, which optimally consider the root distribution of positive and negative sequence components, for μ_{+1} and μ_{-1} are marked in **FIGURE 4**. According to the root locus plots, μ_{+1} is set to 1 (beneficial for the computational burden) which results $\delta = 310.366$ with sampling frequency 12800 Hz and $\tau_{set} = 12.8$ ms. The μ_{-1} is set to 0.7 considering the interaction of fundamental positive sequence and negative sequence components. The value of μ_m is set as $\mu_{+1} / |m|$ where $|m| = 5, 7, 11$ based on two points: 1) this selection is beneficial for reducing computational cost; 2) this selection makes harmonic estimation has the same settling time with fundamental positive sequence components. Furthermore, a generic method is proposed in [28] to tune the parameters by pole placement which allows for an arbitrary design for the dynamic response of dc-offset and harmonic components estimation. If the matrix gains are adopted observers, then the method in [28] will be a good choice for the parameters design.

Based on the selected μ_m , $\sum \mu_m |m| = 4.7\mu_1$. According to Nyquist sampling theorem, the digital angle frequency $|m|\omega T_s$ must be less than π . For the 11-orders harmonic observing in this paper, the limitation $\omega T_s < \pi/11$ is the minimum requirement. In practical case for harmonics detection, more sampling points in one period are required, making the term $\omega T_s \sum \mu_m |m|$ often a small value, such as $\omega T_s \sum \mu_m |m| < 4.7\pi / 110 = 0.134$ in the case of ten points in one period of 11th harmonic. Hence, the division term in (18) can be replaced by Taylor formula:

$$\left(1 + \omega T_s \sum_m \mu_m |m|\right)^{-1} \approx 1 - \omega T_s \sum_m \mu_m |m| + \left(\omega T_s \sum_m \mu_m |m|\right)^2 \quad (22)$$

where the 2-order term can be neglected with acceptable performance of OSPDO.

III. FLL DESIGN

If the IMs have a different frequency parameter than the input signal the output signal recreated by the IMs will not approximate the input signal. Hence, it is necessary to develop a frequency adaptation loop to compute the correct parameter ω of the IMs. This mission can be performed by a FLL.

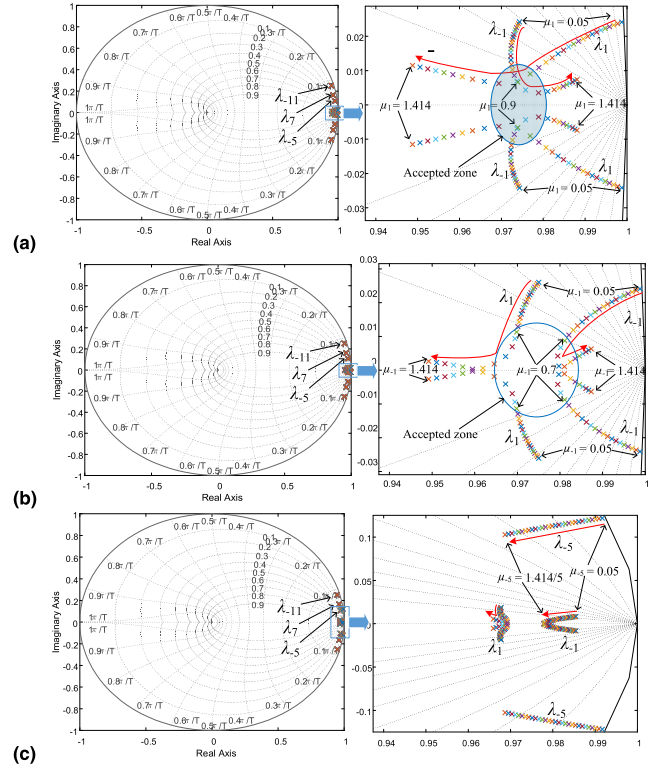


FIGURE 4. Root locus with (a) μ_1 varying and others is set $1/|m|$; (b) μ_{-1} varying and others is set $1/|m|$; (c) μ_{-5} varying and others is set $1/|m|$.

A. FREQUENCY ERROR ANALYSIS

Supposing that the frequency parameter of the DTDMs is $\hat{\omega}$ and considering the fundamental positive sequence condition, the closed-loop dynamic process of the sequence component can be rewritten as

$$\hat{x}_{\alpha\beta,k+1}^{(+1)} = hG(\hat{\omega}T_s)\hat{x}_{\alpha\beta,k}^{(+1)} + (1-h)v_{\alpha\beta,k}^{(+1)} \quad (23)$$

where $h = (1 + \mu\hat{\omega}T_s)^{-1}$. To explicitly illustrate the implicit dynamic process of the frequency error under the estimating, two new state variables are defined:

$$x_{d,k} = v_{\alpha\beta,k}^{(+1)T} \hat{x}_{\alpha\beta,k+1}^{(+1)} \quad (24)$$

$$x_{c,k} = e_k \otimes \hat{x}_{\alpha\beta,k+1}^{(+1)} = v_{\alpha\beta,k}^{(+1)T} \begin{bmatrix} 0 & 1 \\ -1 & 0 \end{bmatrix} \hat{x}_{\alpha\beta,k+1}^{(+1)} \quad (25)$$

where the superscript ‘T’ represents transposition. Utilizing (3) and (23) it has

$$\begin{bmatrix} x_{d,k+1} \\ x_{c,k+1} \end{bmatrix} = hG_e \begin{bmatrix} x_{d,k} \\ x_{c,k} \end{bmatrix} + (1-h) \begin{bmatrix} 1 \\ 0 \end{bmatrix} \|v_{\alpha\beta,k}^{(+1)}\|^2 \quad (26)$$

where $G_e = G(-\omega_e T_s)$ and $\omega_e = \omega - \hat{\omega}$ representing frequency error. From (26), it is clear that $x_{d,k}$ ultimately converges to $\|v^{(+1)} \alpha \beta\|^2$ which is the square of the amplitude of the input positive sequence voltage and $x_{c,k}$ converges to 0 if $\omega_e = 0$.

B. FREQUENCY ESTIMATION

The steady-state value of x_{ck} for the proposed algorithm is:

$$x_{c,\infty} = \frac{-\mu\hat{\omega}T_s v_{\alpha\beta,k}^{(+1)T} v_{\alpha\beta,k}^{(+1)} \sin(\omega_e T_s)}{(1 + \mu\hat{\omega}T_s)^2 - 2(1 + \mu\hat{\omega}T_s) \cos(\omega_e T_s) + 1} \quad (27)$$

Apparently, $x_{c,k}$ carries the frequency error information. To estimate ω , it is necessary to consider that ω is a slow varying direct current signal, namely

$$\omega_{k+1} - \omega_k \approx 0 \quad (28)$$

Consequently, the frequency can be estimated by the adaptive update law

$$\hat{\omega}_{k+1} = \hat{\omega}_k + \Gamma x_{c,k} \quad (29)$$

where $x_{c,k}$ is the correction term, since x_{ck} includes the frequency error formation. The dynamic of ω_e is

$$\omega_{e,k+1} = \omega_{e,k} - \Gamma x_{c,k} \quad (30)$$

which may make ω_e converge to zero if Γ is selected properly.

Assuming that $\hat{\omega}$ is close to ω , then $\sin(\omega_e T_s) \approx \omega_e T_s$, $\cos(\omega_e T_s) \approx 1$ and $v_{\alpha\beta,k}^{(+1)} \approx \hat{x}_{\alpha\beta,k+1}^{(+1)}$. From(27) it can be derived:

$$x_{c,\infty} \approx \frac{-x_{d,\infty} \omega_e T_s}{\mu \hat{\omega} T_s} \approx -\frac{v_{\alpha\beta,\infty}^{(+1)T} \hat{x}_{\alpha\beta,\infty}^{(+1)}}{\mu \hat{\omega}} \omega_e \approx -\frac{\|y_k^{(+1)}\|^2}{\mu \hat{\omega}} \omega_e \quad (31)$$

Considering (31), the gain Γ is set as $\gamma T_s \mu \hat{\omega}_k / \|y_k^{(+1)}\|^2$ to normalize the gain design. Consequently, the dynamic of the frequency estimation can be approximated as

$$\omega_{e,k+1} = \omega_{e,k} + \gamma T_s \omega_{e,k} \quad (32)$$

As long as γ satisfies $|1 + \gamma T_s| < 1$ which yields $\gamma < 0$, ω_{ek} will converge to zero. As a result, (26) will also converge to corresponding $\|v_{\alpha\beta}^{(+1)}\|^2$ and zero. The definition $(1 + \gamma T_s)^{-1} = e^{-\delta \omega T_s}$ is made to approximately tune γ by settling time $\tau_\omega = 4/\delta\omega$.

IV. STABILITY ANALYSIS

First, the input of (26) is $\|v_{\alpha\beta}^{(+1)}\|^2$ which is irrelevant to the frequency error ω_e . Then, considering the Lyapunov function $V = x^T P x$, $P > 0$ and $x = [x_{d,k}, x_{c,k}]^T$, it has

$$\Delta V_k = V_{k+1} - V_k = x^T \left(h^2 G_e^T P G_e - P \right) x \quad (33)$$

Setting $P = I_2$ and $G_e^T G_e = I_2$, where I_2 is a second-order unity matrix, it has $\Delta V_k = (h^2 - 1)x^T x < 0$ which means that the negative definiteness of ΔV_k is independent on ω_e because of the orthogonality of G_e . Therefore, (26) will be stable regardless the value of ω_e , and the stability of (26) is independent on (29). This property is important, because it ensures that provided the frequency estimation loop is stable, then the whole system is stable.

To further analyze the dynamic process of the system when considering the observer and FLL together, the second

TABLE 1. Parameters and signals used in the simulation and experiment.

| Items | Parameters |
|-------------------------|---|
| Proposed | $\mu_{+1} = 1 \mu_{-1} = 0.7 \mu_m = \mu_{+1} / m \omega_c = 100\pi, \gamma = 120$ |
| Method in [13] | $\sigma = 200, \gamma = 19400$ |
| SOGI-FLL | $k = 1.414, \Gamma = 50$ |
| AVF-FLL | $T_\omega = 50 \text{ ms}, k_f = 0.73$ |
| Harmonics in simulation | $v^{(+1)}: 260 \text{ V}, v^{(-1)}: 52 \text{ V}, v^{(-5)}: 78 \text{ V}, v^{(+7)}: 78 \text{ V}, v^{(-11)}: 78 \text{ V}$ |
| Harmonics in experiment | $v^{(+1)}: 160\sqrt{2} \text{ V}, v^{(-1)}: 30\sqrt{2} \text{ V}, v^{(-5)}: 30\sqrt{2}\angle 20^\circ \text{ V}, v^{(+7)}: 50\sqrt{2}\angle 40^\circ \text{ V}, v^{(-11)}: 40\sqrt{2}\angle 40^\circ \text{ V}$ |

equations of (26) and the corresponding counterpart of the proposed FLL and the one in [13] are rewritten as (the definitions of the auxiliary variables are similar with the proposed method):

$$x_{c,k+1} = -hx_{d,k} \sin(\omega_e T_s) + hx_{c,k} \cos(\omega_e T_s) \quad (34)$$

$$x_{c,k+1} = (1 - b)x_{c,k} \cos(\omega_e T_s) + (1 - b)x_{d,k} \sin(\omega_e T_s) - b \sin(\omega_e T_s) \|v_{\alpha\beta,k}^{(+1)}\|^2 \quad (35)$$

where (35) is for the method in [13] and b is the defined parameter in [13]. Considering the first-order approximation of the triangle function and combing (34), (35) and (30), the following error dynamic systems can be deduced to evaluate the performance of the proposed FLL and the one in [13] (36) and (37), as shown at the bottom of the next page:

To analyze the effect of T_s ($1/f_s$) to the system, it is reasonable to consider another parameters invariant. Then, the performance can be simply analyzed by the time-invariant system (36) and (37). The root locus of (36) and (37) with $\gamma = 120$ and $\mu = 1$ are shown in **FIGURE 5**. As shown in **FIGURE 5**, obviously the proposed algorithm has a stronger robustness to the sampling frequency. With the decreasing of the sampling frequency, the damping ratio of the method in [13] reduces faster and ultimately becomes unstable. However, the proposed algorithm remains stable even the sampling frequency reduces to 100 Hz ($n = 2$).

It is worth mentioning that (36) can also be used to tune the parameter γ . It will lead to the similar result with the one tuned by (32), but (36) gives higher accuracy. Furthermore, the effects of other parameters to the system can also be analyzed through (36) and (37) with the same approach (for example the effect of μ to the frequency estimation). Comparing (36) and (37), it is not difficult to predict that the dynamic response of (36) is better than (37). Therefore, the proposed algorithm has the better performance.

V. RESULTS

A. SIMULATION

In this section, some simulations built in MATLAB/Simulink are conducted to demonstrate the excellent characteristics of the proposed method. The parameters are displayed in Table 1.

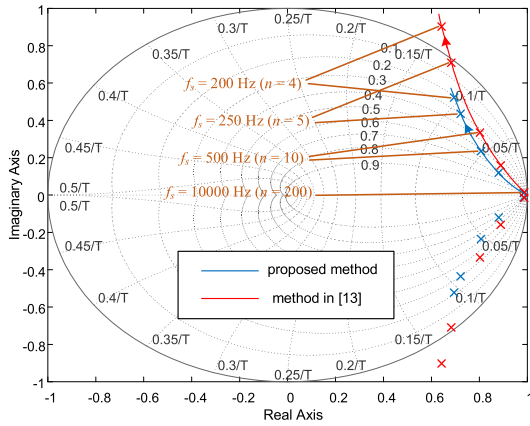


FIGURE 5. Root locus with T_s ($1/f_s$) varying for proposed method and the one in [13].

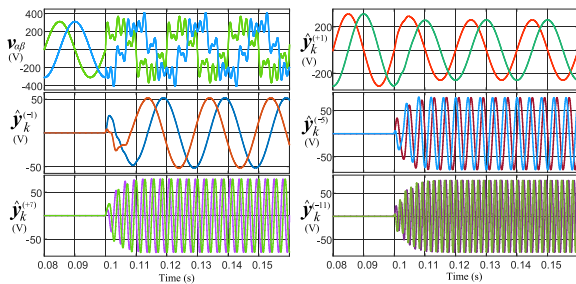


FIGURE 6. Simulation results of the harmonic estimation.

FIGURE 6 displays the results of sequence component estimation without the frequency estimation loop when the input signal $v_{\alpha\beta,k}$ changes from 311 V fundamental positive sequence voltage into a 260 V fundamental positive sequence with different harmonics at 0.1 s. The harmonics are shown in Table 1. Obviously, the estimate results in FIGURE 6 illustrate the excellent filter performance of the proposed OSPDO. The harmonics are successfully detected in about 12 ms. The same distorted three-phase voltage with the voltage presented in FIGURE 6 is used to test the performance of the proposed OSPDO with the frequency estimation loop. The difference is that the frequency changes from 50 Hz to 48 Hz occurs simultaneously at 0.1 s. The simulation results are shown in FIGURE 7. As displayed in FIGURE 7, the proposed OSPDO-FLL gives an excellent dynamic performance. The harmonics are estimated in about 10 ms. And the frequency is estimated successfully within 26 ms within 2% steady-state error. Compared to the results in FIGURE 6, the dynamic response of the OSPDO is slightly affected by the frequency adaptive law.

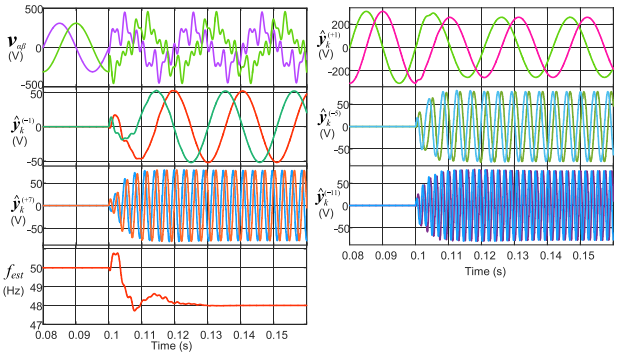


FIGURE 7. Simulation results of the harmonic and frequency estimation.

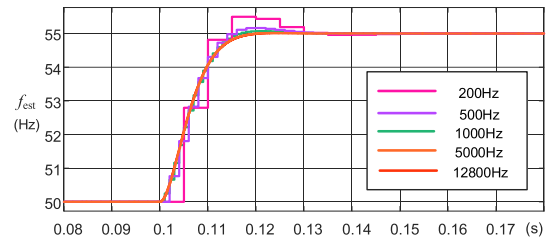


FIGURE 8. Simulation results of frequency estimation of the proposed algorithm with different sampling frequencies.

FIGURE 8 shows the step response of the proposed FLL with different sampling frequency. As predicted in Section III, the results in FIGURE 8 prove that the proposed algorithm has a strong robustness to different sampling frequencies. The ratio of the sampling frequency and the frequency of contained harmonic can achieve a very small value, which means that a low sampling frequency is available when the high-order harmonics need to be addressed for frequency estimating. Moreover, as shown in FIGURE 8 and corresponding to FIGURE 5 with the sampling frequency reducing, the damping ratio is reduced slightly. This verify the correctness of the conclusion in Section III.C.

B. PERFORMANCE COMPARISON

The behavior of the proposed algorithm was tested in a practical test system with a 32-bit TMS320F28335-based control board. In the experiments, the test voltages simulated by a programmable AC source Chroma 61511 were measured and processed by the control board. The result data were exported from the DSP buffer.

The steady-state precision and dynamic response of the frequency estimation for various synchronization methods were experimentally compared. A pure positive sequence

$$\begin{bmatrix} x_{c,k+1} \\ \omega_{e,k+1} \end{bmatrix} = \begin{bmatrix} h & -hx_{d,k}T_s \\ -\Gamma & 1 \end{bmatrix} \begin{bmatrix} x_{c,k} \\ \omega_{e,k} \end{bmatrix} \quad (36)$$

$$\begin{bmatrix} x_{c,k+1} \\ \omega_{e,k+1} \end{bmatrix} = \begin{bmatrix} 1-b & -x_{d,k}T_s + bT_s \left(x_{d,k} - \|v_{\alpha\beta,k}^{(+)}\|^2 \right) \\ -\Gamma & 1 \end{bmatrix} \begin{bmatrix} x_{c,k} \\ \omega_{e,k} \end{bmatrix} \quad (37)$$

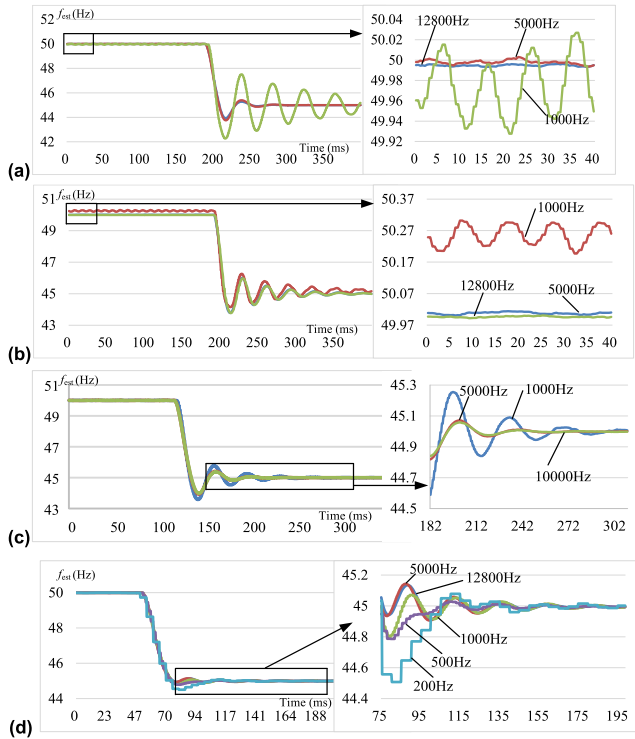


FIGURE 9. Experimental comparison of different algorithms with different sampling frequencies, (a) SOGI-TOI; (b) AVF-TUSTIN; (c) Algorithm in [13] and (d) OSPDO-FLL.

fundamental voltage signal was applied to these methods which include the SOGI discretized by a third order integrator (SOGI-TOI) [4], AVF discretized by Tustin (AVF-TUSTIN) [7], and the proposed algorithm. The parameters of SOGI-based FLL and AVF-based FLL were set according to [10] and [7], respectively. The set of σ and γ for the method in [13] is also based on the guideline stated in [13]. For the proposed algorithm, γ is set to -90 resulting about 44 ms settling time.

The experimental comparison of the proposed algorithm and the existing algorithms from other papers are shown in **FIGURE 9** which verifies the stability analysis in Section III and performance improvements of the proposed algorithm. **FIGURE 9** (a) is based on SOGI-TOI, from which, it can be seen that as the sampling frequency decreased, the performance of SOGI-TOI evidently deteriorated and the steady state error also appeared. The performance of AVF-TUSTIN also deteriorated as displayed in **FIGURE 9** (b). Hence, the observers (SOGI and AVF) designed in continuous domain are not suitable to work in low sampling frequency conditions (less than 2000Hz). Therefore, they also cannot be used to estimate and address the maximum 50-order harmonic with accepted sampling frequencies or cannot apply to the aircraft power system. **FIGURE 9** (c) shows the experimental results of the algorithm proposed in [13]. Although the algorithm proposed in [13] can converge to the real frequency of input signal with sampling frequency of 1000 Hz, the dynamic performance became deteriorated too. The results of the proposed OSPDO-FLL are shown in **FIGURE 9** (d). It shows

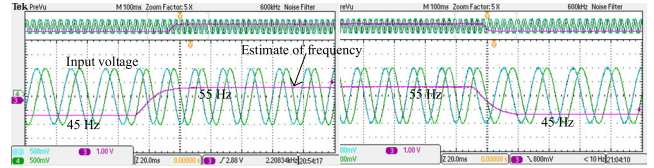


FIGURE 10. Experiment result of frequency jump with different initial values.

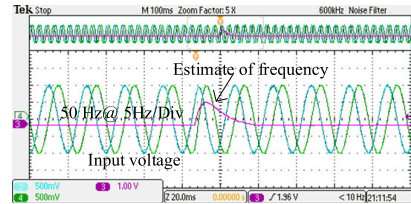


FIGURE 11. Experiment result of 40° phase jump.

that the OSPDO-FLL performs better dynamic response, such as the small oscillation and faster settling time compared to the other synchronization methods. These results also prove the correctness of the conclusion in Section III.C.

Furthermore, the precision of the steady-state frequency estimation was computed through $p\% = (f_{est} - f_{norm}) \times 100 / f_{norm} \%$ where f_{norm} (50Hz) is the nominal frequency of input signal and f_{est} is the steady state estimation value of the synchronization methods. The precisions of the different methods are listed in Table 2. It is obviously to see from Table 2. that the proposed OSPDO-FLL can meet the error criteria (less than 0.03%) of the frequency estimation specified by IEC standard 61000-4-7 [[29]]. Moreover, the lowest ratio of sampling frequency and estimated frequency is decreased to 2. This is meaningful for decreasing the sampling frequency when high-order harmonics exist in the estimated input voltage. To sum up, the proposed algorithm demonstrates performance improvement in both dynamic and steady response on frequency estimation.

C. FREQUENCY AND PHASE JUMP TEST

To further verify the performance of the proposed OSPDO-FLL, the frequency jump with different initial values and phase jump are tested. **FIGURE 10** shows the frequency jumps from 45 Hz to 55 Hz and then returns to 45 Hz. As can be seen in **FIGURE 10**, the proposed OSPDO-FLL performs a good dynamic response for the frequency estimation with different initial values. **FIGURE 11** shows the result of the 40° phase jump. Obviously, the proposed OSPDO-FLL can successfully estimate the frequency in case of the phase jump.

D. ESTIMATION FOR 50th HARMONIC

Based on some standards which require to estimate harmonics up to 50th, the proposed method is used to estimate the high order harmonics under 5000 Hz sampling frequency to highlight its superiority on high-order harmonic estimation. A 36 V 2500 Hz harmonic component was suddenly added

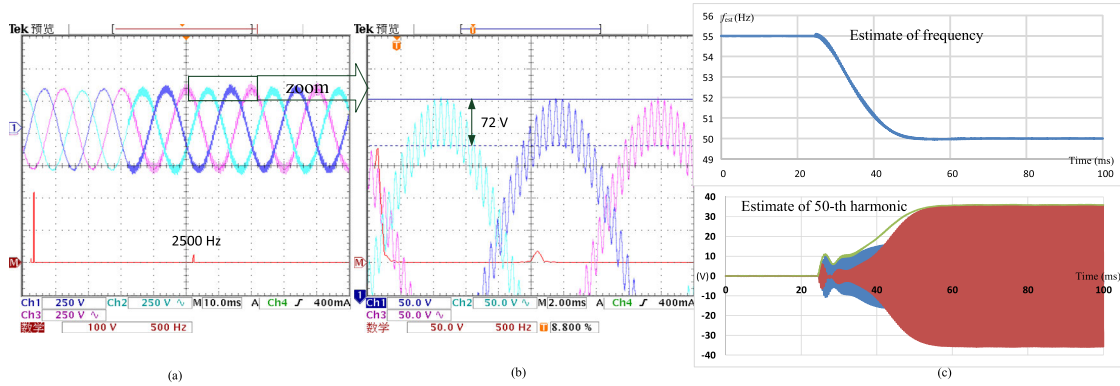


FIGURE 12. Estimation of maximum 2,500 Hz harmonic with 5,000 Hz sampling frequency: (a) input voltage (red line is the FFT); (b) zoom of the input voltage; (c) Top figure: the frequency estimation, bottom figure: estimation of the 50-th harmonic.

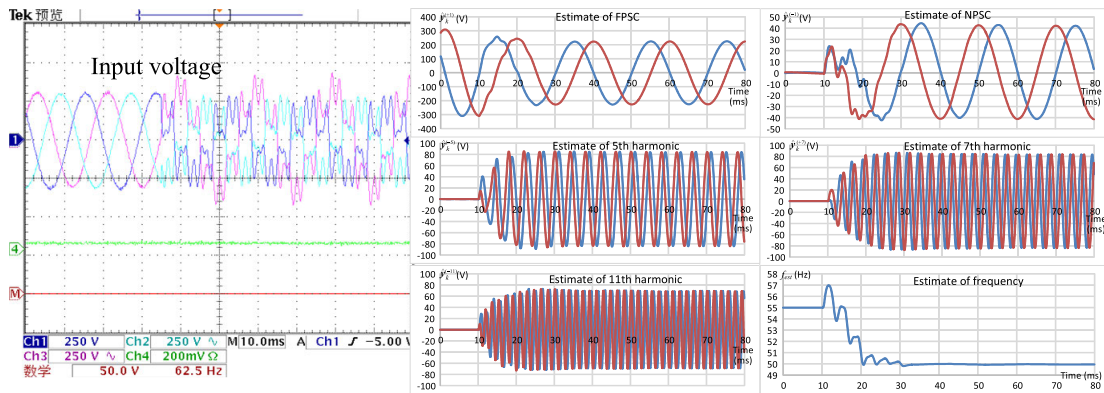


FIGURE 13. Performance of the harmonics detection of OSPDO-FLL when frequency jumps.

TABLE 2. Precision comparison of different algorithms with different sampling frequencies.

| Sampling frequency | Ratio | OSPDO | Method in [13] | SOGI-TOI | AVF-TUSTIN |
|--------------------|-------|-------|----------------|-------------|-------------|
| 12800Hz | 256 | 0.96% | 0.33% | 1.03% | 0.70% |
| 5000 Hz | 100 | 0.38% | 0.33% | 0.40% | 1.74% |
| 1000 Hz | 20 | 0.53% | 0.33% | 5.37% | 5.14% |
| 300 Hz | 6 | 0.35% | instability | instability | instability |
| 200Hz | 4 | 0.34% | instability | instability | instability |
| 100Hz | 2 | 0.33% | instability | instability | instability |

to the fundamental positive sequence component as shown in **FIGURE 12**. Meanwhile, the frequency decreased from 55 Hz to 50 Hz. For the results shown in **FIGURE 1** (c), the green line denotes the amplitude of the 50th harmonic component, while blue and red lines indicate the instantaneous estimated value of the 50th harmonic. The results prove that the estimation performance will not be deteriorated when observing the high order harmonic with a relatively low sampling frequency. The frequency and 50th harmonic can be fast estimated with high precision.

E. HARMONIC DETECTION WITH FREQUENCY VARIATION

To evaluate the performance of the proposed OSPDO-FLL under the severe condition, a test case where the harmonic swells, sags and frequency variation occur simultaneously was carried out. In this test case, the sampling frequency is selected as 12800Hz. And γ is the same with the simulation case. Normally, the system is balanced, hence the $-5, +7, -11$ harmonics are considered. Moreover, in case of the grid fault condition, the unbalanced fundamental component (-1 order) and voltage drop of fundamental positive sequence component will appear, therefore, -1 order component and the voltage drop on $+1$ order component are considered in the test case. The harmonics sequence components are shown in Table 1. Meanwhile, the frequency experiences 5 Hz sudden decrease (from 55 Hz to 50 Hz).

FIGURE 13 shows the input voltage, observed sequence components and estimated frequency. As shown in **FIGURE 13**, it can be found that all the sequence components are observed successfully with good dynamic performance as well as the frequency. In such a severe condition, the frequency estimation only takes about 22 ms and performs good transient response. The fast response is useful for the grid-tied inverter control where the fast transient response is often required to deal with the grid variations.

TABLE 3. Computation complexity and time comparison of different algorithms for positive and negative sequence fundamental component observation.

| Item method | Shift | '+' & 'x' | sin & cos | '+' & 'x' | sin & cos | time |
|----------------|-------|-----------|-----------|-----------|-----------|--------------|
| OSPDO | 4 | 24 | 2 | 24 | 2 | 2.01 μ s |
| SOGI-TOI | 16 | 48 | x | 48 | x | 4.24 μ s |
| Method in [13] | 4 | 27 | 2 | 27 | 2 | 2.06 μ s |
| AVF-TUSTIN | 12 | 36 | x | 36 | x | 3.28 μ s |

F. COMPUTATIONAL BURDEN

In the digital control system of a power converter, the computational resource is critical for the implementation of digital control. Hence, the computation complexity and burden are investigated to value the superiority of the proposed OSPDO-FLL. The computation complexity of SOGI [9], [10] and AVF [7] highly depends on the discretization method, while the proposed OSPDO-FLL does not have this issue. In order to get a straightforward sight on the computation complexity and burden differences, the conventional SOGI-TOI, AVF-TUSTIN, the algorithm in [13] and the proposed OSPDO are compared in Table 3. The results listed in Table 3 are consumed for positive and negative sequence fundamental components observation. It can be observed from Table 3 that not only the proposed OSPDO is simple to implement but it also consumes the least computational burden and resource of DSP. All the harmonics were estimated in 5.41 μ s and the whole OSPDO-FLL took 6.29 μ s (for the test case in).

VI. CONCLUSION

This paper established a one-step-prediction discrete observer (OSPDO) which is appropriate for the observation of harmonic sequence components for three-phase systems, especially for the application of low sampling frequency. Based on the OSPDO, the frequency error is analyzed and then a discrete frequency-locked-loop (OSPDO-FLL) is designed and analyzed.

The algorithm is designed in discrete domain so that the performance degradation and estimation error introduced by the discretization process can be avoided. Moreover, the proposed OSPDO-FLL demonstrates an excellent steady and dynamic performance, such as the high estimating precision for frequency and fast dynamic response. Furthermore, the proposed state space analysis method also reveals that the proposed algorithm has strong robustness to sampling frequency, which means the algorithm is more suitable to estimate high order harmonics and apply to aircraft power system compared to existed algorithms. Because it can be implemented with a relatively low sampling frequency but without deteriorating the performance.

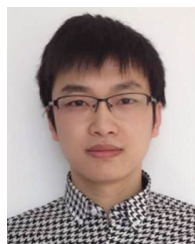
REFERENCES

- [1] S. Golestan, J. M. Guerrero, and J. C. Vasquez, "Three-phase PLLs: A review of recent advances," *IEEE Trans. Power Electron.*, vol. 32, no. 3, pp. 1894–1907, Mar. 2017.
- [2] S. Golestan, J. M. Guerrero, J. C. Vasquez, A. M. Abusorrah, and Y. Al-Turki, "A study on three-phase FLLs," *IEEE Trans. Power Electron.*, vol. 34, no. 1, pp. 213–224, Jan. 2019.
- [3] P. Rodriguez, J. Pou, J. Bergas, J. I. Candela, R. P. Burgos, and D. Boroyevich, "Decoupled double synchronous reference frame PLL for power converters control," *IEEE Trans. Power Electron.*, vol. 22, no. 2, pp. 584–592, Mar. 2007.
- [4] M. Ciobotaru, R. Teodorescu, and F. Blaabjerg, "A new single-phase PLL structure based on second order generalized integrator," in *Proc. IEEE PESC*, Jun. 2006, pp. 1511–1516.
- [5] P. Lin, Y. Shi, and X.-M. Sun, "A classes of nonlinear active disturbance rejection loop filters for phase-locked loop," *IEEE Trans. Ind. Electron.*, early access, May 25, 2021, doi: 10.1109/TIE.2021.3060663.
- [6] S. Golestan, J. M. Guerrero, J. C. Vasquez, A. M. Abusorrah, and Y. Al-Turki, "Linear time-periodic modeling, examination, and performance enhancement of grid synchronization systems with DC component rejection/estimation capability," *IEEE Trans. Power Electron.*, vol. 36, no. 4, pp. 4237–4253, Apr. 2021, doi: 10.1109/TPEL.2020.3018584.
- [7] S. Vazquez, J. A. Sanchez, M. R. Reyes, J. I. Leon, and J. M. Carrasco, "Adaptive vectorial filter for grid synchronization of power converters under unbalanced and/or distorted grid conditions," *IEEE Trans. Ind. Electron.*, vol. 61, no. 3, pp. 1355–1367, Mar. 2014.
- [8] X. Quan, X. Dou, Z. Wu, M. Hu, and A. Q. Huang, "Complex-coefficient complex-variable filter for grid synchronization based on linear quadratic regulation," *IEEE Trans. Ind. Informat.*, vol. 14, no. 5, pp. 1824–1834, May 2018, doi: 10.1109/TII.2017.2761834.
- [9] P. Rodríguez, A. Luna, R. S. Muñoz-Aguilar, I. Etxeberria-Otadui, R. Teodorescu, and F. Blaabjerg, "A stationary reference frame grid synchronization system for three-phase grid-connected power converters under adverse grid conditions," *IEEE Trans. Power Electron.*, vol. 27, no. 1, pp. 99–112, Jan. 2012.
- [10] P. Rodriguez, A. Luna, I. Candela, R. Mujal, R. Teodorescu, and F. Blaabjerg, "Multiresonant frequency-locked loop for grid synchronization of power converters under distorted grid conditions," *IEEE Trans. Ind. Electron.*, vol. 58, no. 1, pp. 127–138, Jan. 2011.
- [11] G. Fedele and A. Ferrise, "A frequency-locked-loop filter for biased multi-sinusoidal estimation," *IEEE Trans. Signal Process.*, vol. 62, no. 5, pp. 1125–1134, Mar. 2014.
- [12] C. M. Hackl and M. Landerer, "Modified second-order generalized integrators with modified frequency locked loop for fast harmonics estimation of distorted single-phase signals," *IEEE Trans. Power Electron.*, vol. 35, no. 3, pp. 3298–3309, Mar. 2020, doi: 10.1109/TPEL.2019.2932790.
- [13] S. Gomez Jorge, C. A. Busada, and J. A. Solsona, "Frequency adaptive discrete filter for grid synchronization under distorted voltages," *IEEE Trans. Power Electron.*, vol. 27, no. 8, pp. 3584–3594, Aug. 2012.
- [14] S. G. Jorge, J. A. Solsona, and C. A. Busada, "Sequences detection of an unbalanced sinusoidal voltage of unknown frequency using a reduced-order observer," *IEEE Trans. Power Del.*, vol. 28, no. 3, pp. 1499–1507, Jul. 2013.
- [15] X. He, H. Geng, and G. Yang, "Reinvestigation of single-phase FLLs," *IEEE Access*, vol. 7, pp. 13178–13188, 2019, doi: 10.1109/ACCESS.2019.2891973.
- [16] X. Quan, Q. Hu, X. Dou, Z. Wu, and W. Li, "High-order frequency-locked loop: General modeling and design," *IEEE Trans. Ind. Electron.*, early access, Dec. 3, 2020, doi: 10.1109/TIE.2020.3040688.
- [17] X. Quan and A. Q. Huang, "PI-based synchronous reference frame frequency-locked loop," *IEEE Trans. Ind. Electron.*, vol. 68, no. 5, pp. 4547–4553, May 2021, doi: 10.1109/TIE.2020.2985002.
- [18] Z. Dai, P. Zhao, X. Chen, M. Fan, and J. Zhang, "An enhanced transfer delay-based frequency locked loop for three-phase systems with DC offsets," *IEEE Access*, vol. 7, pp. 40380–40387, 2019, doi: 10.1109/ACCESS.2019.2903581.
- [19] J. Geng, X. Li, Q. Liu, J. Chen, Z. Xin, and P. Chiang Loh, "Frequency-locked loop based on a repetitive controller for grid synchronization systems," *IEEE Access*, vol. 8, pp. 154861–154870, 2020, doi: 10.1109/ACCESS.2020.3018639.
- [20] A. G. Yepes, F. D. Freijedo, J. Doval-Gandoy, Ó. López, J. Malvar, and P. Fernandez-Comesaña, "Effects of discretization methods on the performance of resonant controllers," *IEEE Trans. Power Electron.*, vol. 25, no. 7, pp. 1692–1712, Jul. 2010.
- [21] F. Tedesco, A. Casavola, and G. Fedele, "Discrete-time frequency-locked-loop filters for parameters estimation of sinusoidal signals," in *Proc. 52nd IEEE Conf. Decis. Control*, Dec. 2013, pp. 4399–4404.

- [22] F. J. Rodriguez, E. Bueno, M. Aredes, L. G. B. Rolim, F. A. S. Neves, and M. C. Cavalcanti, "Discrete-time implementation of second order generalized integrators for grid converters," in *Proc. 34th Annu. Conf. IEEE Ind. Electron.*, Orlando, FL, USA, Nov. 2008, pp. 176–181.
- [23] X. Quan, X. Dou, Z. Wu, M. Hu, and F. Chen, "A concise discrete adaptive filter for frequency estimation under distorted three-phase voltage," *IEEE Trans. Power Electron.*, vol. 32, no. 12, pp. 9400–9412, Dec. 2017, doi: [10.1109/TPEL.2017.2657641](https://doi.org/10.1109/TPEL.2017.2657641).
- [24] *IEEE Recommended Practices and Requirements for Harmonic Control in Electrical Power Systems*, Standard 519, 2014.
- [25] F. Cupertino, E. Lavopa, P. Zanchetta, M. Sumner, and L. Salvatore, "Running DFT-based PLL algorithm for frequency, phase, and amplitude tracking in aircraft electrical systems," *IEEE Trans. Ind. Electron.*, vol. 58, no. 3, pp. 1027–1035, Mar. 2011.
- [26] S. Golestan, J. M. Guerrero, and J. C. Vasquez, "Is using a complex control gain in three-phase FLLs reasonable?" *IEEE Trans. Ind. Electron.*, vol. 67, no. 3, pp. 2480–2484, Mar. 2020, doi: [10.1109/TIE.2019.2903748](https://doi.org/10.1109/TIE.2019.2903748).
- [27] C. M. Hackl and M. Landerer, "A unified method for online detection of phase variables and symmetrical components of unbalanced three-phase systems with harmonic distortion," *Energies*, vol. 12, no. 17, p. 3243, Aug. 2019, doi: [10.3390/en12173243](https://doi.org/10.3390/en12173243).
- [28] C. Hackl and M. Landerer, "A unified method for generic signal parameter estimation of arbitrarily distorted single-phase grids with DC-offset," *IEEE Open J. Ind. Electron. Soc.*, vol. 1, pp. 235–246, 2020, doi: [10.1109/OJIES.2020.3017379](https://doi.org/10.1109/OJIES.2020.3017379).
- [29] *Testing and Measurement Techniques-General Guide on Harmonics and Interharmonics Measurements and Instrumentation, for Power Supply Systems and Equipment Connected Thereto*, Standard 61000-4-7, IEC, 2002.



FAN YANG was born in Liaoning, China, in 1982. He is currently a Senior Engineer with the Electric Power Research Institute, State Grid Hubei Electric Power Company. His current research interests include distribution network optimized operation and maintenance.



XIANGJUN QUAN (Member, IEEE) received the B.S.E.E. degree in electrical engineering from Chongqing University, Chongqing, China, in 2007, and the M.S. and Ph.D. degrees in electrical engineering from Southeast University, Nanjing, China, in 2011 and 2018, respectively. From February 2017 to August 2017, he had studied with FREEDM, NC State University. From September 2017 to August 2018, he had also studied with the University of Texas at Austin as an Exchange Student. He was a Research and Development Engineer with Huawei Technologies, from 2011 to 2012. Since 2018, he has been an Assistant Professor with Southeast University. His current research interests include digital control technique for converters, renewable energy generation systems, and microgrid.



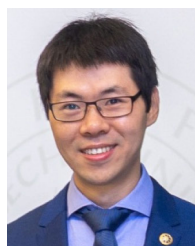
WEI HU was born in Anhui, China, in 1981. She is currently a Senior Engineer with the Electric Power Research Institute, State Grid Hubei Electric Power Company. Her current research interests include distribution network planning and operation analysis.



FUJIN DENG (Senior Member, IEEE) received the B.S. degree in electrical engineering from the China University of Mining and Technology, Jiangsu, China, in 2005, the M.S. degree in electrical engineering from Shanghai Jiao Tong University, Shanghai, China, in 2008, and the Ph.D. degree in energy technology from the Department of Energy Technology, Aalborg University, Aalborg, Denmark, in 2012. He joined as a Professor with the School of Electrical Engineering, Southeast University, Nanjing, China, in 2017. From 2013 to 2015, he was a Postdoctoral Researcher with the Department of Energy Technology, Aalborg University. From 2015 to 2017, he was an Assistant Professor with the Department of Energy Technology, Aalborg University. His main research interests include wind power generation, multilevel converters, high-voltage direct-current technology, DC grid, and offshore wind farm-power systems dynamics.



YAODONG WU is currently pursuing the bachelor's degree in electrical engineering and its automation with Southeast University, Nanjing, China. His research interests include inertia-supported modeling analysis of power systems under new energy generation and optimal control design of inverters.



ZHIXIANG ZOU (Senior Member, IEEE) received the B.Eng. and Ph.D. degrees in electrical engineering from Southeast University, Nanjing, China, in 2007 and 2014, respectively, and the Dr.-Ing. degree (*summa cum laude*) from Kiel University, Germany. He was an Engineer with the State Grid Electric Power Research Institute, Nanjing, from 2007 to 2009. He was a Research Fellow with the Chair of Power Electronics, Kiel University, from 2014 to 2019. He is currently an Associate Professor with the School of Electrical Engineering, Southeast University. His research interests include smart transformers, microgrid stability, modeling, and control of power converters. He serves as an Associate Editor for the IEEE OPEN JOURNAL OF POWER ELECTRONICS and IEEE ACCESS and an Editor for the *International Transactions on Electrical Energy Systems* and the *Mathematical Problem in Engineering*.



YU SHEN was born in Hubei, China, in 1983. He is currently a Senior Engineer with the Electric Power Research Institute, State Grid Hubei Electric Power Company. His current research interests include distribution network planning and distribution network optimized operation and maintenance.

...